Nanoscale

PAPER

Cite this: *Nanoscale*, 2021, **13**, 14973

Nanocomplex made up of antimicrobial metallo-supramolecules and model biomembranes – characterization and enhanced fluorescence†

Chung-Hao Liu,[a] Heng Wang,[b] Lin Yang,[c] Yun Liu,[d,e] Xiaopeng Li [b] and Mu-Ping Nieh *[a,f]

Received 23rd June 2021,
Accepted 30th July 2021

DOI: 10.1039/d1nr04083a

rsc.li/nanoscale

Antimicrobial pentatopic 2,2′:6′,2″-terpyridines that form 3-D supramolecular hexagonal prisms with Cd^{2+} through coordination driven self-assembly can be entrapped by lipid discoidal bicelles, composed of 1,2-dipalmitoyl-*sn-glycero*-3-phosphocholine, 1,2-dihexanoyl-*sn-glycero*-3-phosphocholine and 1,2-dipalmitoyl-*sn-glycero*-3-phospho-(1′-rac-glycerol) lipid, forming a well-defined nanocomplex. Structural characterization performed by very small angle neutron scattering, small angle X-ray scattering and transmission electron microscopy suggests that the hexagonal prisms are preferably located at the rim of bicellar discs with the hexagonal face in parallel with the bilayers, instead of face-to-face stacking. Such a configuration reduces the π–π interaction and consequently enhances the fluorescence emission. Since novel supramolecules were reported to have antibiotic functions, this study provides insight into the interactions of antimicrobial supermolecules with lipid membranes, leading to potential theranostic applications.

Introduction

Recently, rational design of novel 3-D supramolecules with well-defined cavities, constructed by coordination-driven self-assembly, has attracted substantial attention in the supramolecular fields. They provide great potential for the development of the desired supramolecules for many applications in sensing,[1] optoelectronic devices,[2] drug delivery,[3] and artificial transmembrane channels.[4] A recently designed 3-D hexagonal prism (**HP**) synthesized from pentatopic 2,2′:6′,2″-terpyridine (P-TPY) with three different environments (Fig. 1, TPY^{a-c})[5] shows potential antimicrobial activities against two Gram-positive bacteria, including MRSA and *Bacillus subtilis* (*B. subtilis*), leading to a potential solution for the emergent challenge of shortage of antibodies. However, the **HP** dissolves only in organic solvents, *i.e.*, acetone nitrate, methanol (MeOH), or dimethyl sulfoxide (DMSO), which are not ideal candidates for biological use. Overcoming the challenge of biocompatibility and understanding the interactions between the supramolecules and biomembranes are important factors for *in vivo* administration of the **HP**. This report therefore focuses on the structural characterization of a **HP**/lipid nanocomplex, which greatly enhances the aqueous solubility as well as provides insight into the interaction of the **HP** with biomembranes.

In the past, biocompatible lipid systems showed the capability of entrapping hydrophobic molecules. One example is the discoidal bicellar system,[6–9] composed of long-chain (L) lipids, *e.g.*, dipalmitoylphosphatidylcholine (DPPC, di-C_{16}PC) and dipalmitoylphosphatidylgylcerol (DPPG, di-C_{16}PG), and short-chain (S) lipids, *e.g.*, dihexanoyl phosphatidylcholine (DHPC, di-C_6PC), with molar ratios in the range of $2 \leq [L]/[S] \leq 5$.[6] The formation mechanism of nanodiscs is attributed to the hydrophobic interaction, immiscibility between S and L lipids, appropriate molecular spontaneous curvatures (one planar and the other rim) and sufficient surface charged density.[6] Such nanodiscs generally yield uniform radii (10–15 nm) and bilayer thickness (~5 nm). Most intriguingly, they demonstrate 5–10 times enhancement of cellular uptake compared with the vesicles of the same chemical compositions.[7,8] Hence, bicelles can be an ideal nanocarrier platform for the **HP**, not only

[a]*Polymer Program, Institute of Material Science, University of Connecticut, Storrs, Connecticut 06269, USA. E-mail: mu-ping.nieh@uconn.edu*
[b]*College of Chemistry and Environmental Engineering, Shenzhen University, Shenzhen 518055, China*
[c]*National Synchrotron Light Source – II, Brookhaven National Laboratory, Upton, New York 11973, USA*
[d]*Center for Neutron Research, National Institute of Standards and Technology, Gaithersburg, Maryland 20899, USA*
[e]*Chemical & Biomolecular Engineering Department, University of Delaware, Newark, Delaware 19716, USA*
[f]*Department of Chemical and Biomolecular Engineering, University of Connecticut, Storrs, Connecticut 06269, USA*
†Electronic supplementary information (ESI) available. See DOI: 10.1039/d1nr04083a

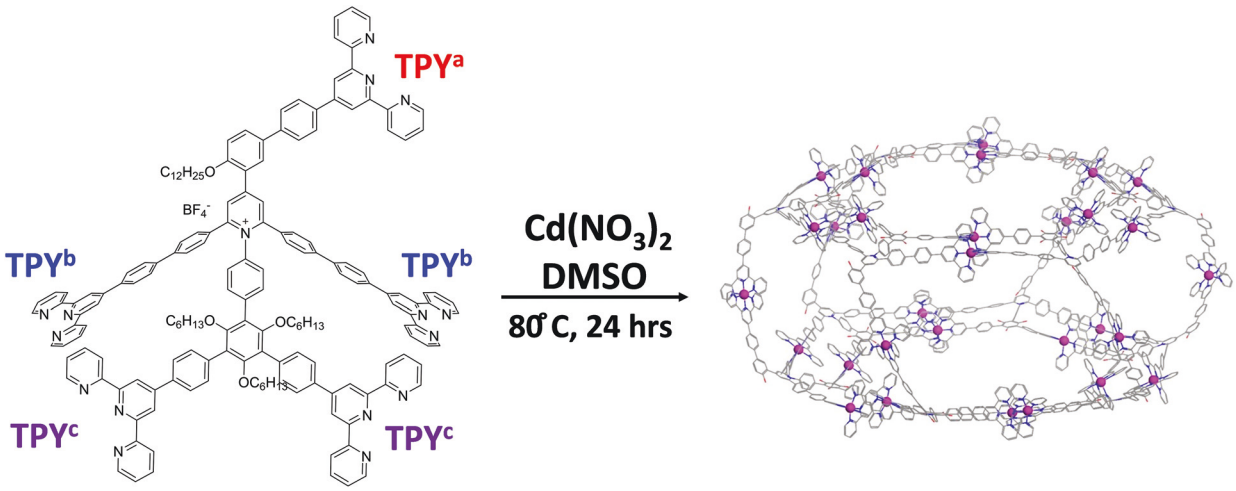

Fig. 1 The 3-D chemical structure of the **HP** self-assembly, where the alkyl chains are omitted for clarity.

enhancing the solubility in biologically relevant aqueous solution but also increasing the endocytosis of the **HP**.

From the transmission electron microscopy (TEM) and small angle scattering (SAS) data, we found that the **HP** can be successfully encapsulated in bicelles around the rim. Another intriguing discovery is that the enhancement of fluorescence emission intensity is observed as the **HP** is loaded in bicelles compared with the free **HP** in an organic solvent, showing aggregation enhanced emission (AEE) as reported recently.[10,11]

Results and discussion

HP structure characterization

Fig. 1 shows the proposed drum-like structure of **HP** self-assemblies through the designed coordination with Cd^{2+}. The dimensions of the **HP** self-assemblies in deuterated DMSO are characterized by best fitting the very small angle neutron scattering (vSANS) data with a core–shell cylinder model, as shown in Fig. S4 and Table S1.† The best fit yields a radius, a shell thickness and a drum height of 2.3, 1.5 and 2.7 nm, respectively (ESI†) consistent with the previous report.[5] In order to encapsulate **HP** self-assemblies in the lipid bilayer without imposing high stress on the biomembrane, at least one of the dimensions should be less than the bilayer thickness. The free **HP** self-assembly seems to satisfy the condition based on the structural characterization.

Encapsulation efficiency (EE)

Since **HP** is practically insoluble in water, the preparation of **HP**-loaded bicelles (**HP-B**) was achieved by the dispersed **HP** and lipids in $CHCl_3$ and MeOH mixtures. The samples were then redispersed in water after being dried. The **HP** can be loaded in the lipid self-assemblies through the hydrophobic interaction. Centrifugation was applied to remove the non-encapsulated **HP**, yielding yellowish **HP-B**.

The quantity of the encapsulated **HP** can be determined from the pre-calibrated UV-vis absorption spectra, where the absorption is linearly dependent on the concentration of **HP** (Fig. S5†). Fig. 2 shows the EE% of the **HP**-to-lipid molar ratio of 1 : 3140 and 1 : 1470. The sample with a **HP**-to-lipid ratio of 1 : 3140 has an EE% of 78% ± 10%, which drastically decreases to 15% ± 8% for the higher **HP**-to-lipid ratio (1 : 1047) sample due to the fact that the sample of the high **HP**-to-lipid ratio destabilized the discoidal structure of the nanocomplex into vesicles (Fig. S6†). Therefore, our analysis mainly focuses on the 1 : 3140 **HP-B**.

Absorption and emission spectrum

Fig. 3(a) shows the UV-vis absorption of the pristine bicelles (**PB**), 1 : 3140 **HP-B** and free **HP**, respectively. The **PB** illustrates no absorbance in the probing range of wavelength. For comparison purposes, the absorption spectrum of **HP-B** is normal-

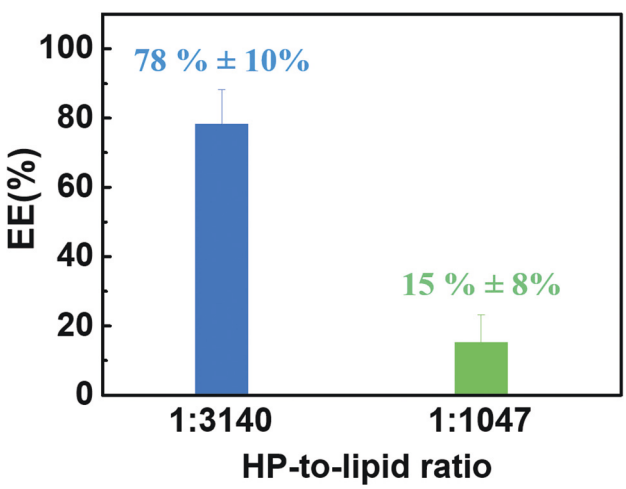

Fig. 2 The EE% of samples with the HP-to-lipid ratios of 1 : 3140 and 1 : 1047, yielding the results of (78% ± 10%) and (15% ± 8%), respectively.

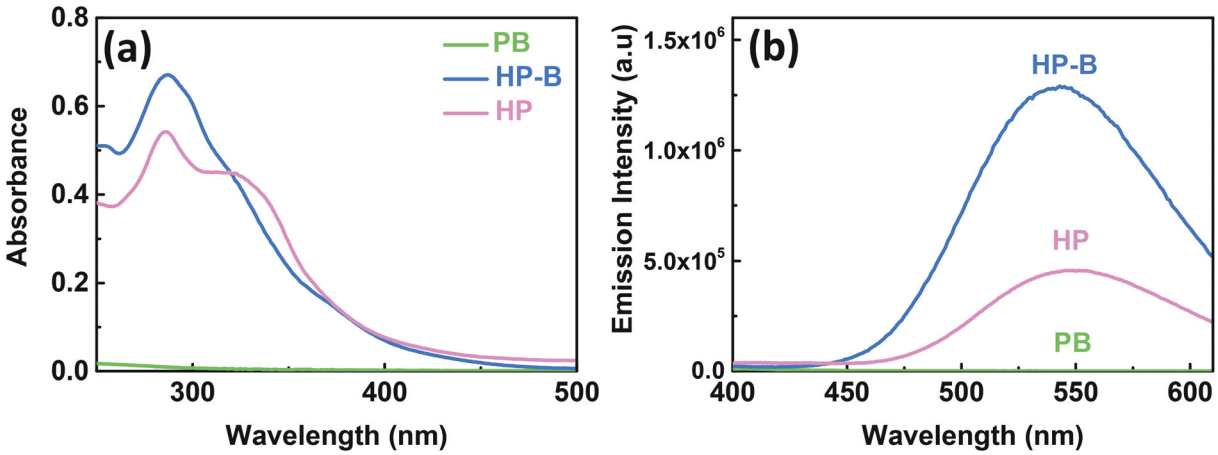

Fig. 3 (a) The UV-vis absorption and (b) emission spectra (λ_{ex} = 320 nm) of PB, HP-B and HP.

ized according to EE%. The absorption spectra of **HP-B** (in aqueous solution) and free **HP** (in $CHCl_3$/MeOH) exhibit a maximum peak at 286 nm from the pentatopic TPY ligands (P-TPY). The absorption peak slightly shifts from 291 nm to 286 nm (Fig. S7†). The phenomenon is also observed when ligands coordinate with Zn(II)[12] and Cd(II)[13] to form metallo-supramolecules. The shoulder peak for free **HP** at around 320 nm may result from $\pi \rightarrow \pi^*$ due to the supramolecular stacking (π–π interaction)[13,14] of a tubular-like self-assembling structure of **HPs** in an organic solvent.[5,15] The reduced absorbance of 320 nm of the **HP-B** suggests weaker π–π interactions.[13,14] As the **HP-B** was dried and redispersed into the mixture of $CHCl_3$/MeOH, the absorption spectrum was found identical to that of free **HP** (Fig. S8†), indicating the same drum-like structure of **HP**. It should be noted that drum-like **HP** *only* forms in an organic solvent (*e.g.*, DMSO) at 80 °C for 12 hours (Fig. 1). The fact that the drying process and re-dispersion in $CHCl_3$/MeOH were conducted at 50 °C and room temperature, respectively, suggests that it is unlikely for the **HP** to dissociate after encapsulation in the first place and then assemble into a drum-like structure again.

The **HP** exhibits fluorescence with the maximum emission wavelength, λ_{em} of 550 nm (at λ_{ex} = 320 nm) as shown in Fig. 3(b). Like most of the organic fluorophores, the normalized emission intensity of "free" **HP** decreases with increased **HP** concentrations (Fig. S9†). The highest normalized emission intensity was found at the lowest **HP** concentration, due to the aggregation-caused quenching (ACQ) effect, presumably due to the preferable base-to-base self-assembly by π–π interactions.[5,16,17] Intriguingly, the **HP-B** (1 : 3140) emits a three-fold intensity compared to the free **HP** solution at the same concentration [Fig. 3(b)]. However, 1 : 1047 **HP-B** shows less emission (Fig. S10†) due to either low EE% or morphological disruption (Fig. S6†). The emission peak slightly shifts from 550 nm to 543 nm [Fig. 3(b)] possibly because of the fewer π–π interactions in **HP-B** as π–π interaction is expectedly leading to the red shift of fluorescence.[18–20] The emission enhancement in conjunction with the blue shift suggests

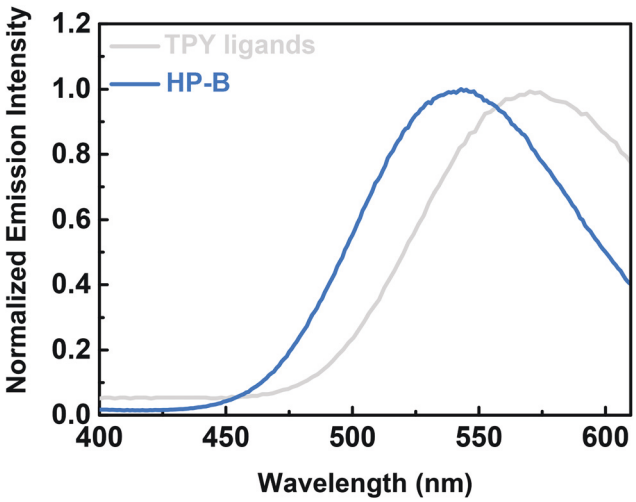

Fig. 4 The fluorescence spectra of pentatopic TPY ligands (λ_{ex} = 280 nm), and HP-B (λ_{ex} = 320 nm). The intensity is normalized by peak intensity for clarity of the peak position.

reduced base-to-base configuration. Another possible explanation would be the restricted intramolecular motion (RIM) as the **HP** is confined in the bicelles causing the so-called aggregation-enhanced emission (AEE).[10,20] Most importantly, the different emission spectra between **HP-B** and metal-free P-TPY as shown in Fig. 4 suggests that the **HP** likely retains the 3D drum-like structure after encapsulation.

Structural characterization of the HP-B

The morphology of **HP-B** and the location of the **HP** in the bicelles reveal the interactions between the **HP** and lipids. Both TEM micrographs of the **PB** and **HP-B** indicate that nanodiscs are retained regardless of the encapsulation of the **HP**. However, the **PB** are overall smaller with an average diameter of ~16.8 (± 4.5) nm [Fig. 5(a) and (b)], consistent with the literature values,[6] while the **HP-B** yields larger discs with an average diameter of 30.6 (± 7.8) nm [Fig. 5(d) and (e)]. The

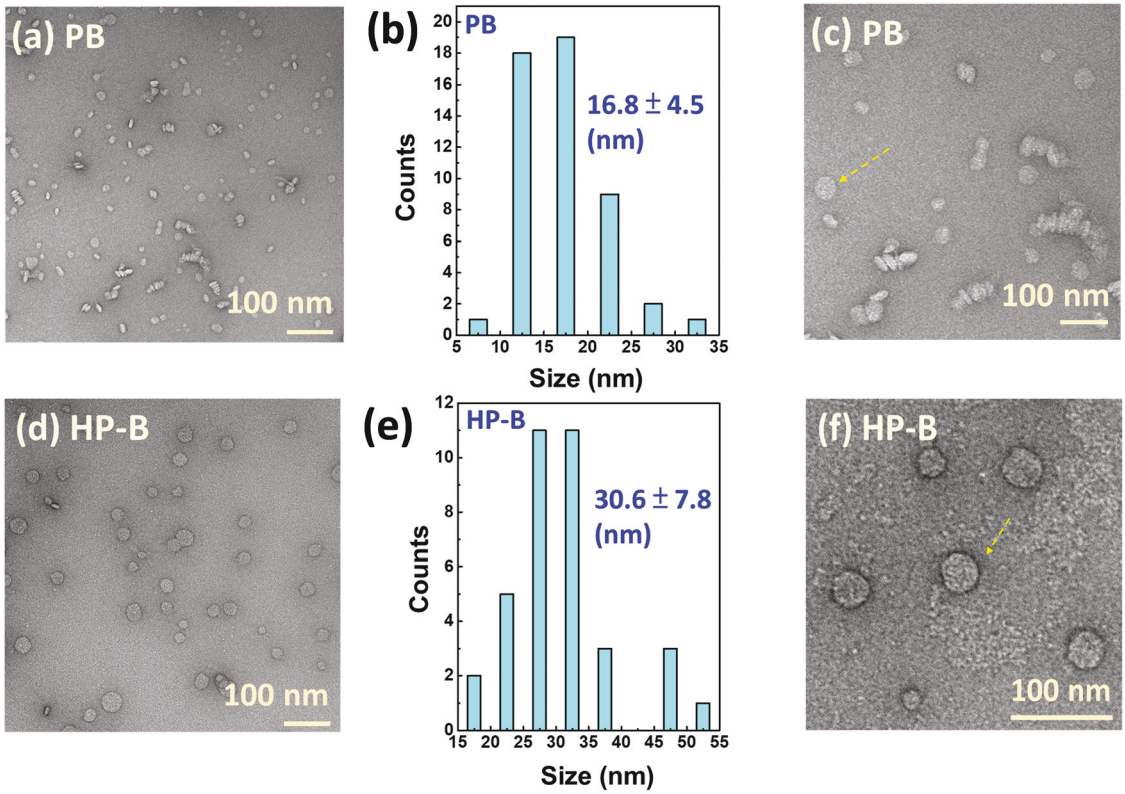

Fig. 5 (a), (c) and (d), (f) are TEM images of **PB** and **HP-B**, respectively, on the same copper grids at different locations. (b) and (e) are the diameter distributions of **PB** and **HP-B**, which are obtained *via* Image J, respectively. The yellow arrows in (c) and (f) show higher electron densities of the rim of the **HP-B** in comparison with that of the **PB**.

darker rim of **HP-B** [Fig. 5(c) and (f)] implies that the encapsulated **HP** (with higher electron density) may preferably locate at the rim of bicelles. The internal structure of **HP-B** can be revealed by vSANS using the DPPG, deuterated DPPC-d_{62} and DHPC-d_{35} with the average neutron scattering length density (NSLD), ρ_{lipid} of 5.12 × 10^{-6} Å^{-2} in a null-contrast solvent at D_2O/H_2O = 82/18, where $\rho_{solvent}$ equals ρ_{lipid}.[21] The contrast between the protiated **HP** and the remaining components is therefore enhanced as shown in Fig. S11.† As the vSANS data (Fig. S12†) can be fitted by a core–shell discoidal model (CSD, Fig. S2†), the best fitting parameters (Table S2†) show a decreased rim NSLD presumably due to the lower NSLD of the protiated **HP**, indicating that **HP**s preferably situate themselves at the rim, in good agreement with the TEM results. Furthermore, the hydrophobic thickness (L_{length}) of the bicellar planar region is in the range between 37 Å and 39 Å (Table S2†) with minimal dependence of **HP**-loading, suggesting that **HP** is unlikely inserted in the bilayer.

SAXS can also provide structural information of **HP-B** as the phosphate groups of lipids and the middle of the bilayer, respectively, have the highest and lowest electron density across the bilayer, rendering three significant broad peaks in the range of scattering vector, q between 0.05 and 0.5 Å^{-1}. A five-layer core shell discoidal model (5LCSD), instead of the CSD model, was used to fit the SAXS data to reveal the detailed internal bilayer structure with the lengths and electron densities of methylene and methyl regimes [Fig. 6(a)].[22] Fig. 6(b) shows the reduced SAXS data and their best fits. The Hayter–Penfold model (structure factor), which is commonly used for describing interparticle coulombic repulsion, is required for interpreting the low-q intensity with a peak at ~0.015 Å^{-1} for the **PB**, while no structural factor is required for **HP-B** presumably due to larger interparticle spacing with larger discs. Two of the high-q peaks at 0.27 Å^{-1} and 0.405 Å^{-1} slightly move to 0.28 Å^{-1} and 0.425 Å^{-1}, respectively, after the loading of the **HP** [Fig. 6(c)] indicates subtle structural changes. The best fitting results (Table 1) show that the core radius of **HP-B** increases from 83 (±1) Å to 319 (±11) Å and the rim thickness, T_r, also increases from 47 (± 27) Å to 204 (± 6) Å, agreeing with the TEM and vSANS analyses which show the entrapped **HP** preferably located at the rim, leading to a larger T_r. The outcome is consistent with a previous report of hydrophobic gold nanoclusters entrapped at the bicellar rim, which is mainly made of fluidic DHPC in the L_α phase.[23–25]

Thermal analysis of HP-B

Fig. 7(a) and (b) show the DSC thermograms of **PB** and 1 : 3140 **HP-B** with 0.1 wt% of lipid concentration. For **PB** [Fig. 7(a)], the peaks at 41 and 45 °C correspond to the melting transition temperature (T_m) of DPPC and bicelle-to-vesicle transformation, respectively.[26] The identical thermogram on the second-time temperature (T)scan suggests reversibility of the bicelle-

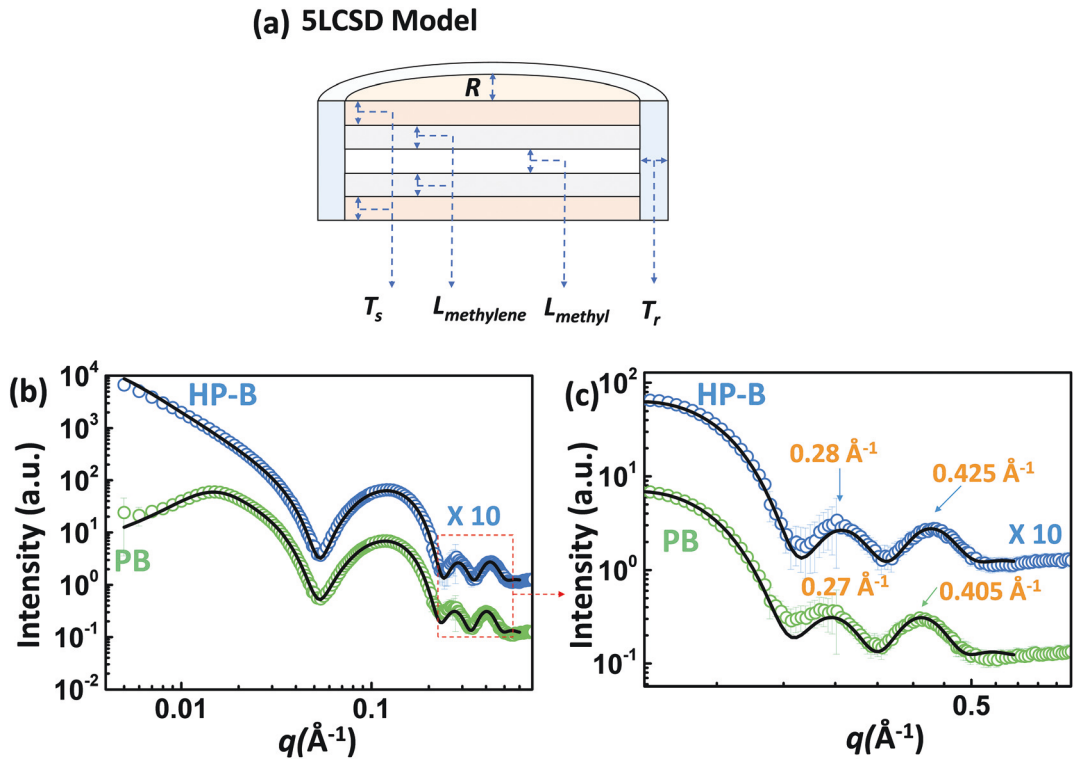

Fig. 6 (a) The cross-section of the 5LCSD model. (b) 1-D SAXS results of **PB** (green) and **HP-B** (blue). (c) The blowup of the dashed box in (b) with a zoomed-in view. The data of **HP-B** is scaled by 10 for clarity.

Table 1 The best-fitted results of the **PB** and **HP-B** based on the SAXS data

Parameters/samples	PB	HP-B
Core radius (Å)	83 ± 1	319 ± 11
T_r (Å)	47 ± 27	204 ± 6
$L_{methylene}$ (Å)	13 ± 0.2	12 ± 0.3
L_{methyl} (Å)	11 ± 0.5	9 ± 0.6
$\rho_{methylene}$ (10^{-6}/Å^2)	9.47 ± 0.01	9.47 ± 0.01
ρ_{methyl} (10^{-6}/Å^2)	8.76 ± 0.02	8.72 ± 0.03
ρ_{rim} (10^{-6}/Å^2)	9.47 ± 0.01	9.50 ± 0.01

to-vesicle structural transformation of **PB** in contrast to the previous reports, which show irreversibility of the structural transformation after the 2nd thermal cycles.[26–28] The main reason is that the applied higher charge density (R = 0.05) of **PB** stabilizes the discoidal structure.[21] The DSC thermograms of **HP-B**, however, show irreversibility of the bicelle-to-vesicle transformation after the first thermal cycling, similar to the irreversible behavior in the weakly charged systems, where high-T vesicle retains after being cooled down. We thus

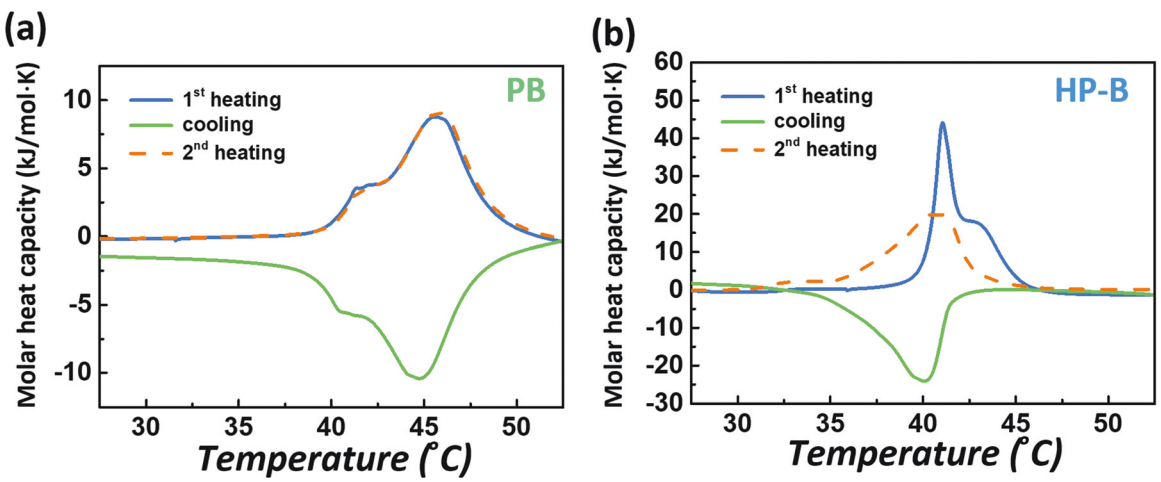

Fig. 7 DSC thermograms of (a) the **PB** and (b) the **HP-B** undergoing a heating–cooling-heating process.

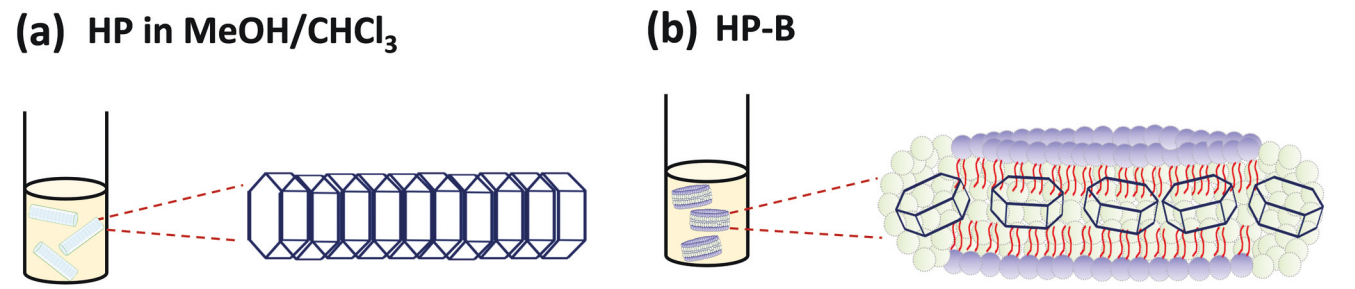

Fig. 8 The schematics of **HP** conformations in (a) organic solvent and (b) bicelles.

hypothesize that the entrapment of the **HP** destabilizes the discoidal morphology. Another interesting observation is that the enthalpy to melt gel-DPPC (the area underneath the 41 °C peak) of the **HP-B** is found significantly higher than that of **PB**. This suggests that more DHPC is driven to the rim to shield **HP**, resulting in greater segregation between DPPC and DHPC, yielding a higher quantity of the gel phase and consequently larger discs, consistent with the TEM and SAXS outcomes.

The previous report revealed that the **HP** adopted the base-to-base stacking [Fig. 8(a)] in an organic solvent.[5] Since the diameter of the **HP** "drum" is found to be 7.6 nm, which is larger than two-fold of the bilayer hydrophobic thickness (~3.7 nm), it is not feasible to maintain the same aggregation behavior in the bicelles. Less energy is expected to encapsulate HP in the bicelles when the hexagonal face of the **HP** orients parallel with the bilayer as shown in Fig. 8(b). Such molecular arrangement reduces the π–π interaction, which agrees well with the observation of blue-shifted fluorescence spectra and consequently shows the enhancement in emission as described previously.

Conclusions

We have confirmed that the hydrophobic drum-like self-assembled supramolecule, **HP**, can be encapsulated in uniform-sized discoidal bicelles forming a well-defined nanoframe-in-nanodisc complex. Such one-pot synthesis with high EE (~78%) greatly enhances the concentration of the **HP** dispersed in aqueous solutions. All experimental evidence suggests that the **HP** preferably locates at the high-curvature rim made of the DHPC, allowing interactions with hydrophobic molecules.[24,25,29] Moreover, the **HP-B** exhibits three-fold emission intensity compared with that of the free **HP** in the organic solvent, presumably because the entrapped **HP** self-assembles reducing the base-to-base stacking. Instead, they may be packed at the rim parallel to the bilayer. The UV-vis and fluorescence spectra show that the **HP** likely maintains a drum shape in the interior of the bicelles.

The **HP-B** platform further increases the biocompatibility and solubility in aqueous solution, making its antimicrobial function more applicable for the *in vivo* study. The enhancement of emission also makes it a potential candidate for theranostic purposes. Furthermore, this study further provides insight into understanding the structure–function relationship of supramolecules interacting with biomembranes.

Disclaimer

Access to vSANS was provided by the Center for High Resolution Neutron Scattering, a partnership between the National Institute of Standards and Technology and the National Science Foundation under Agreement no. DMR-2010792. Certain commercial equipment, instruments, or materials (or suppliers, or software) are identified in this paper to foster understanding. Such identification does not imply recommendation or endorsement by the National Institute of Standards and Technology, nor does it imply that the materials or equipment identified are necessarily the best available for the purpose.

Author contributions

C.-H. L., performed the experiments, analyzed data, and wrote the manuscript. H. W. and X. Li. designed and synthesized the supramolecule, **HP**. L. Y. and Y. L. are the beamline scientists at the Brookhaven National Lab and National Institute of Standards and Technology. M.-P. N. supervised the entire project. All authors reviewed, edited and approved the manuscript prior to submission.

Conflicts of interest

The authors declare no conflicts of interest.

Acknowledgements

The authors are grateful for the beamtime at the LiX beamline[30,31] of NSLS-II (Brookhaven National Lab) through a beamtime proposal (BAG-302208). The LiX beamline is part of the Center for BioMolecular Structure (CBMS), primarily sup-

ported by the National Institutes of Health, National Institute of General Medical Sciences through a Center Core P30 Grant (P30GM133893), and by the DOE Office of Biological and Environmental Research (KP1607011), with additional support from the NIH Grant S10OD012331. NSLS-II is a U.S. Department of Energy (DOE) Office of Science User Facility operated for the DOE Office of Science by Brookhaven National Laboratory under Contract no. DE-SC0012704. Access to vSANS was provided by the Center for High Resolution Neutron Scattering, a partnership between the National Institute of Standards and Technology and the National Science Foundation under Agreement no. DMR-2010792.

References

1 L. E. Kreno, K. Leong, O. K. Farha, M. Allendorf, R. P. Van Duyne and J. T. Hupp, *Chem. Rev.*, 2012, **112**, 1105–1125.
2 C. Wang, D. Liu and W. Lin, *J. Am. Chem. Soc.*, 2013, **135**, 13222–13234.
3 Y.-R. Zheng, K. Suntharalingam, T. C. Johnstone and S. J. Lippard, *Chem. Sci.*, 2015, **6**, 1189–1193.
4 C. J. E. Haynes, J. Zhu, C. Chimerel, S. Hernández-Ainsa, I. A. Riddell, T. K. Ronson, U. F. Keyser and J. R. Nitschke, *Angew. Chem., Int. Ed.*, 2017, **56**, 15388–15392.
5 H. Wang, C.-H. Liu, K. Wang, M. Wang, H. Yu, S. Kandapal, R. Brzozowski, B. Xu, M. Wang, S. Lu, X.-Q. Hao, P. Eswara, M.-P. Nieh, J. Cai and X. Li, *J. Am. Chem. Soc.*, 2019, **141**, 16108–16116.
6 Y. Liu, Y. Xia, A. T. Rad, W. Aresh and M.-P. Nieh, in *Liposomes: Methods and Protocols*, ed. G. G. M. D'Souza, Springer New York, New York, NY, 2017, pp. 273–282, DOI: 10.1007/978-1-4939-6591-5_22.
7 W. Aresh, Y. Liu, J. Sine, D. Thayer, A. Puri, Y. Huang, Y. Wang and M. P. Nieh, *J. Biomed. Nanotechnol.*, 2016, **12**, 1852–1863.
8 A. T. Rad, C. W. Chen, W. Aresh, Y. Xia, P. S. Lai and M. P. Nieh, *ACS Appl. Mater. Interfaces*, 2019, **11**, 10505–10519.
9 A. T. Rad, S. Malik, L. Yang, T. K. Oberoi-Khanuja, M.-P. Nieh and R. Bahal, *Nanoscale*, 2019, **11**, 12517–12529.
10 J. Luo, Z. Xie, J. W. Y. Lam, L. Cheng, H. Chen, C. Qiu, H. S. Kwok, X. Zhan, Y. Liu, D. Zhu and B. Z. Tang, *Chem. Commun.*, 2001, 1740–1741, DOI: 10.1039/B105159H..
11 B. Z. Tang, X. Zhan, G. Yu, P. P. S. Lee, Y. Liu and D. Zhu, *J. Mater. Chem.*, 2001, **11**, 2974–2978.
12 P. Narea, J. Cisterna, A. Cárdenas, P. Amo-Ochoa, F. Zamora, C. Climent, P. Alemany, S. Conejeros, J. Llanos and I. Brito, *Polymers*, 2020, **12**, 1756.
13 H. Wang, X. Qian, K. Wang, M. Su, W.-W. Haoyang, X. Jiang, R. Brzozowski, M. Wang, X. Gao, Y. Li, B. Xu, P. Eswara, X.-Q. Hao, W. Gong, J.-L. Hou, J. Cai and X. Li, *Nat. Commun.*, 2018, **9**, 1815.
14 J. Hermann, D. Alfè and A. Tkatchenko, *Nat. Commun.*, 2017, **8**, 14052.
15 C. Wei, Y. He, X. Shi and Z. Song, *Coord. Chem. Rev.*, 2019, **385**, 1–19.
16 G.-Q. Yin, H. Wang, X.-Q. Wang, B. Song, L.-J. Chen, L. Wang, X.-Q. Hao, H.-B. Yang and X. Li, *Nat. Commun.*, 2018, **9**, 567.
17 J. Mei, Y. Hong, J. W. Y. Lam, A. Qin, Y. Tang and B. Z. Tang, *Adv. Mater.*, 2014, **26**, 5429–5479.
18 X. Cao, L. Meng, Z. Li, Y. Mao, H. Lan, L. Chen, Y. Fan and T. Yi, *Langmuir*, 2014, **30**, 11753–11760.
19 X. Cao, Y. Li, A. Gao, Y. Yu, Q. Zhou, X. Chang and X. Hei, *J. Mater. Chem. C*, 2019, **7**, 10589–10597.
20 J. Li, J. Wang, H. Li, N. Song, D. Wang and B. Z. Tang, *Chem. Soc. Rev.*, 2020, **49**, 1144–1172.
21 M.-P. Nieh, C. J. Glinka, S. Krueger, R. S. Prosser and J. Katsaras, *Biophys. J.*, 2002, **82**, 2487–2498.
22 C. Cheu, L. Yang and M.-P. Nieh, *Chem. Phys. Lipids*, 2020, **231**, 104945.
23 M. Kranenburg and B. Smit, *J. Phys. Chem. B*, 2005, **109**, 6553–6563.
24 H. Sharma and E. E. Dormidontova, *ACS Nano*, 2017, **11**, 3651–3661.
25 A. T. Rad, Y. Bao, H.-S. Jang, Y. Xia, H. Sharma, E. E. Dormidontova, J. Zhao, J. Arora, V. John, B. Tang, T. Dainese, A. Hariri, J. Jokerst, F. Maran and M.-P. Nieh, *Adv. Funct. Mater.*, 2020, 2009750.
26 I. Alahmadi, D. Hoy, A. T. Rad, S. Patil, A. Alahmadi and M.-P. Nieh, *Langmuir*, 2021, (under revision).
27 M.-P. Nieh, V. A. Raghunathan, S. R. Kline, T. A. Harroun, C.-Y. Huang, J. Pencer and J. Katsaras, *Langmuir*, 2005, **21**, 6656–6661.
28 M.-P. Nieh, P. Dolinar, N. Kučerka, S. R. Kline, L. M. Debeer-Schmitt, K. C. Littrell and J. Katsaras, *Langmuir*, 2011, **27**, 14308–14316.
29 Y. Xia, H.-S. Jang, Z. Shen, G. D. Bothun, Y. Li and M.-P. Nieh, *Langmuir*, 2017, **33**, 5745–5751.
30 L. Yang, S. Antonelli, S. Chodankar, J. Byrnes, E. Lazo and K. Qian, *J. Synchrotron Radiat.*, 2020, **27**(3), 804–812.
31 L. Yang, E. Lazo, J. Byrnes, S. Chodankar, S. Antonelli and M. Rakitin, *J. Synchrotron Radiat.*, 2021, **28**(4), 1237–1244.